

X-ray Properties of Lyman Break Galaxies in the Great Observatories Origins Deep Survey

B. D. Lehmer,¹ W. N. Brandt,¹ D. M. Alexander,² F. E. Bauer,² C. J. Conselice,³ M. E. Dickinson,⁴ M. Giavalisco,⁵ N. A. Grogin,⁶ A. M. Koekemoer,⁵ K. S. Lee,^{5,6} L. A. Moustakas,⁵ & D. P. Schneider¹

ABSTRACT

We constrain the X-ray emission properties of Lyman break galaxies (LBGs) at $z \approx 3\text{--}6$ using the ≈ 2 Ms *Chandra* Deep Field-North and ≈ 1 Ms *Chandra* Deep Field-South. Large samples of LBGs were discovered using *HST* as part of the Great Observatories Origins Deep Survey (GOODS). Deep optical and X-ray imaging over the GOODS fields have allowed us to place the most significant constraints on the X-ray properties of LBGs to date. Mean X-ray properties of 449, 1734, 629, and 247 LBGs with $z \sim 3, 4, 5$, and 6, respectively, were determined using stacking techniques. When stacked, we detect X-ray emission from LBGs at $z \sim 3$ ($\sim 7\sigma$) and from an optically bright subset (brightest 25%) of LBGs at $z \sim 4$ ($\sim 3\sigma$); the latter is the highest redshift detection yet for “normal” galaxies in the X-ray band. The effective exposure times for these stacked observations are ≈ 0.7 and 0.5 Gs, respectively. The derived average rest-frame 2.0–8.0 keV luminosities are 1.5 and 1.4×10^{41} erg s $^{-1}$, respectively. X-ray emission from these LBGs is likely due to high mass X-ray binaries (HMXBs) and Type II supernovae; the corresponding star formation rates are $\approx 85\text{--}240 M_{\odot}$ yr $^{-1}$. The X-ray to *B*-band mean luminosity ratio (L_X/L_B) at $z \sim 3$ is somewhat elevated with respect to that measured for starburst galaxies in the local Universe (significance $\sim 3\sigma$). When stacking full samples of LBGs at $z \sim 4, 5$, and 6 we do not obtain significant detections ($< 3\sigma$) and derive rest-frame 2.0–8.0 keV luminosity upper limits (3σ) of 0.9, 2.8, and 7.1×10^{41} erg s $^{-1}$, respectively. These upper limits constrain any widespread AGN activity in these objects to be modest at best. Furthermore, we find that $\sim 0.5\%$ of our LBGs from $z \approx 3\text{--}6$ are detected individually in the X-ray band. These LBGs have spectral shapes and luminosities characteristic of moderate-power AGN (e.g., Seyfert galaxies and quasars).

Subject headings: cosmology: observations — cosmology: surveys — X-rays: galaxies — X-rays: general

¹Department of Astronomy & Astrophysics, 525 Davey Lab, The Pennsylvania State University, University Park, PA 16802.

²Institute of Astronomy, Madingley Road, Cambridge, CB3 0HA, United Kingdom.

³Palomar Observatory, California Institute of Technology, Pasadena, CA 91125

⁴NOAO, 950 N. Cherry Ave., Tucson AZ 85719

⁵Space Telescope Science Institute, 3700 San Martin Drive, Baltimore, MD 21218

⁶Johns Hopkins University, 3400 North Charles Street, Baltimore, MD 21218-2686

1. Introduction

Determination of the basic X-ray properties of “normal” (i.e., not hosting a luminous AGN) galaxies out to high redshift has been motivated in part by Ghosh & White (2001, hereafter GW01) who developed a model of the evolution of X-ray luminosity with redshift. GW01 predict that, globally, X-ray emission from normal galaxies should peak at $z \approx 1.5\text{--}3$ due to a maximum in the global star formation rate (SFR) at $z \approx 2.5\text{--}3.5$ (e.g., Blain et al. 1999). Heightened X-ray emission at these redshifts is expected due to an increase in the global population of low mass X-ray binaries (LMXBs). LMXBs evolve on timescales of ~ 1 Gyr, and therefore their X-ray signatures should lag behind more immediate tracers of star formation.

Stacking analyses and deep X-ray surveys with the *Chandra X-ray Observatory* (hereafter *Chandra*) have enabled testing of these predictions out to cosmologically interesting distances. Stacking techniques generally involve the addition of X-ray counts at known positions of galaxies to yield average X-ray detections where individual sources lie below the detection threshold. For example, Hornschemeier et al. (2002, hereafter H02) used stacking with a ≈ 1 Ms exposure of the *Chandra* Deep Field-North (CDF-N) to investigate the evolution of the X-ray luminosities of $z = 0.4\text{--}1.5$ spiral galaxies. This analysis shows suggestive evidence for evolution in X-ray luminosity with redshift at a level somewhat lower than that predicted by GW01. H02 also found that the X-ray to *B*-band luminosity ratio, L_X/L_B , is elevated for $z \approx 1$ spirals with rest-frame $L_B \approx L_B^*$ as compared with galaxies in the local Universe. L_X/L_B has been shown to be linked to star formation activity. This is supported by the existence of an empirical correlation between L_X/L_B and $L_{60\,\mu\text{m}}/L_{100\,\mu\text{m}}$ (Fabbiano & Shapley 2002). Here, the quantity $L_{60\,\mu\text{m}}/L_{100\,\mu\text{m}}$ is a measure of far infrared color temperature, which has been shown to increase with star formation activity (e.g., Helou, Ryter, & Soifer 1991). More recent stacking analyses of large samples of galaxies in the ≈ 2 Ms CDF-N and ≈ 1 Ms *Chandra* Deep Field-South (CDF-S) show that the X-ray properties of normal galaxies of all morphological types evolve similarly from $z = 0.4\text{--}1.5$ (Wu et al. 2004).

At higher redshifts ($z \approx 2\text{--}6$) stacking analyses have been performed using individually undetected normal galaxies (e.g., Brandt et al. 2001, hereafter B01; Nandra et al. 2002, hereafter N02; Malhotra et al. 2003; Bremer et al. 2004; Moustakas & Immler 2004; Reddy & Steidel 2004; Wang et al. 2004). At $z \sim 3$ these galaxies often have mean X-ray luminosities and L_X/L_B comparable to bright starburst galaxies in the local Universe. The heightened X-ray emission from these galaxies is probably due to newly formed high mass X-ray binaries (HMXBs) and young supernova remnants. HMXBs have much shorter formation timescales than LMXBs and are therefore more immediate tracers of cosmic star formation history.

Recently, large samples of galaxies have been identified at $z \sim 3, 4, 5$, and 6 as part of the Great Observatories Origins Deep Survey (GOODS). These galaxies were isolated via the Lyman break technique (e.g., Steidel et al. 1995; Madau et al. 1996; Steidel et al. 1999), which estimates the redshift of a galaxy based on its “dropout” bandpass (see § 2.1). Lyman break galaxies (LBGs) generally show rest-frame UV/optical characteristics similar to those of local starburst galaxies—weak or absent Lyman α emission, P Cygni features from C IV and other lines, and strong interstellar UV absorption lines such as Si II, O I, C II, Si IV, and Al II (see e.g., Steidel et al. 1996; Shapley et al. 2003). The GOODS covers ≈ 316 arcmin 2 of sky in two fields, GOODS-North (GOODS-N) and GOODS-South (GOODS-S) (Giavalisco et al. 2004a). Both

fields are subregions of the *Chandra* Deep Fields for which *Chandra* has acquired an ≈ 2 Ms observation of the CDF-N (Alexander et al. 2003a, hereafter A03) and an ≈ 1 Ms observation of the *Chandra* Deep Field-South (CDF-S; Giacconi et al. 2002; A03).

In this paper, we use stacking techniques to constrain the X-ray properties of LBGs in the GOODS fields. We improve on results from B01 and N02 by increasing the number of galaxies at $z \sim 3$ from 24 (B01) and 148 (N02) to 449, and we add to this samples of 1734, 629, and 247 galaxies at $z \sim 4, 5$, and 6, respectively.

The Galactic column densities are $1.3 \times 10^{20} \text{ cm}^{-2}$ (Lockman 2003) and $8.0 \times 10^{19} \text{ cm}^{-2}$ (Stark et al. 1992) for the CDF-N and CDF-S, respectively. $H_0 = 70 \text{ km s}^{-1} \text{ Mpc}^{-1}$, $\Omega_m = 0.3$, and $\Omega_\Lambda = 0.7$ are adopted throughout this paper (Spergel et al. 2003). Coordinates are J2000.0.

2. Analysis

2.1. Samples

The Lyman break technique has been utilized in the GOODS regions, where deep mosaic images have been taken using the *HST* Advanced Camera for Surveys (ACS) with bandpasses B_{435} , V_{606} , i_{775} , and z_{850} (Giavalisco et al. 2004b, hereafter G04); the full-depth, five-epoch ACS images have been used here. Additional ground-based photometry has been obtained over the GOODS fields in the U band at KPNO (Capak et al. 2004, GOODS-N) and CTIO (GOODS-S). Identification of these LBGs is based on the following color equations:

U -dropouts:

$$\begin{aligned} (U - B_{450}) &\geq 0.75 + 0.5(B_{450} - z_{850}) \wedge \\ (U - B_{450}) &\geq 0.9 \wedge (B_{450} - z_{850}) \leq 4.0 \end{aligned} \quad (1)$$

B_{435} -dropouts:

$$\begin{aligned} (B_{450} - V_{606}) &\geq 1.2 + 1.4 \times (V_{606} - z_{850}) \wedge \\ (B_{450} - V_{606}) &\geq 1.2 \wedge (V_{606} - z_{850}) \leq 1.2 \end{aligned} \quad (2)$$

V_{606} -dropouts:

$$\begin{aligned} [(V_{606} - i_{775}) &> 1.5 + 0.9 \times (i_{775} - z_{850})] \vee \\ [(V_{606} - i_{775}) &> 2.0] \wedge (V_{606} - i_{775}) \geq 1.2 \wedge \\ (i_{775} - z_{850}) &\leq 1.3 \wedge \text{S/N}(B_{450}) < 2.0 \end{aligned} \quad (3)$$

i_{775} -dropouts:

$$\begin{aligned} (i_{775} - z_{850}) &\geq 1.3 \wedge \\ \text{S/N}(B_{450}) &< 2.0 \wedge \text{S/N}(V_{606}) < 2.0 \end{aligned} \quad (4)$$

Here the symbols \wedge and \vee correspond to the logical operators AND and OR, respectively. Monte Carlo simulations of the color-selection procedure (e.g., G04) indicate that these color criteria select galaxies with mean redshifts and 1σ redshift ranges of $z = 3.01 \pm 0.24$, 3.78 ± 0.34 , 4.92 ± 0.33 , and 5.74 ± 0.36 for U -, B_{435} -, V_{606} -, and i_{775} -dropouts, respectively. Dropout lists created in G04 were inspected and filtered to minimize the number of interlopers and contaminants in the samples. The interloper fraction is predicted to be $\approx 10\%$ for U -dropouts and B_{435} -dropouts. This fraction increases to become significant for V_{606} -dropouts and i_{775} -dropouts ($\approx 20\%$ and 40% , respectively; see Dickinson et al. 2004; G04).

The LBGs used in our stacking analyses have average redshifts and z_{850} magnitudes as shown in Figure 1; for comparison the z_{850} magnitudes of several other stacking analyses in this redshift range are also plotted. Galaxies in this survey probe relatively faint optical fluxes over a wider range of redshifts ($z \approx 3\text{--}6$) than those used for previous X-ray stacking analyses. The corresponding lookback times for U -, B_{435} -, V_{606} -, and i_{775} -dropouts are 11.5, 12.1, 12.5, and 12.7 Gyr, respectively (see Hogg 2000).

The stacking procedure used in our analyses was similar to that of B01 and N02; the intent was to obtain average X-ray properties (e.g., luminosities and spectral shapes). At each LBG position, photon counts and effective exposure times (from exposure maps, which include the effects of vignetting) were extracted from circular apertures and summed to give a total number of counts and a total effective exposure time. We excluded LBGs located within $10''$ of individually detected X-ray sources in A03; this avoids contamination by unrelated sources. This exclusion process led to the rejection of 99, 267, 127, and 31 U -, B_{435} -, V_{606} -, and i_{775} -dropouts, respectively ($\approx 18\%$, 13% , 17% , and 11% of the respective LBG populations). A small number of LBGs (18) were found to be within the positional errors of *Chandra* sources; their characteristics are given in § 3.1 and listed in Table 1.

The background was estimated through Monte Carlo analysis using a background map (see § 4.2 of A03). Each LBG position was shifted randomly within $25''$ of the original position, and background counts were obtained for each new position and summed just as they were for the LBGs themselves. This procedure was repeated 10,000 times to obtain an accurate estimate of the local background and its dispersion. To verify our results were not biased by gradients in the local background, we also tried shifting in regions with radii of $10''$, $15''$, $20''$, $30''$, and $35''$ and found no material differences in our results.

Our stacking procedure maximized the signal-to-noise ratio (hereafter, S/N)¹ by varying the aperture cell size for extracting X-ray counts and the off-axis angle (angle between a particular source and the average CDF-N or CDF-S aim points) within which sources were included in stacking. This procedure was performed using U -dropouts because of their strong X-ray signal. We avoided stacking sources that were outside a certain off-axis angle due to the increased size of the point-spread function (PSF) and confusion with background in this region. In the maximization process we chose a specific aperture cell size and stacked sources within various off-axis angles (hereafter, inclusion radii) until S/N was maximized. Sources within the resulting inclusion radius were then stacked using variable aperture cell sizes. S/N was maximized

¹Here, $S/N \equiv (S-B)/B^{0.5}$, where S is the source plus background counts and B is the average background counts obtained from the Monte Carlo procedure. This approximation is accurate for $|S-B| \ll B$ and $B \geq 20$, which applies to all cases in our analyses.

for a specific aperture cell size, and the process was repeated iteratively until convergence. Figures 2a and 2b show the result of this process. We found that S/N peaks for an inclusion radius ≈ 9.0 and an aperture size of $\approx 1.5''$ (as expected for small off-axis angles); these values are used throughout our analyses.

Mean count rates Φ were calculated by subtracting our best estimate of the local background counts B from the background plus source counts S and dividing by the total effective exposure time T [i.e., $\Phi = (S - B)/T$]. To convert count rate to flux we used the Galactic column densities discussed in § 1 and adopted a power-law photon index of $\Gamma = 2.0$, appropriate for starburst galaxies (e.g., Kim, Fabbiano, & Trinchieri 1992; Ptak et al. 1999). Sources were stacked in both the GOODS-N and GOODS-S fields, so we used a statistically weighted Galactic column density. X-ray luminosities were calculated following Schmidt & Green (1986):

$$L_X = 4\pi d_L^2 f_X (1+z)^{\Gamma-2} \text{ erg s}^{-1} \quad (5)$$

where d_L is the luminosity distance (cm), and f_X is the X-ray flux ($\text{erg cm}^{-2} \text{ s}^{-1}$).

2.2. Subsets

The large number of LBGs in our sample enabled investigation of the contribution of specific subsets to the signal. We chose to divide the original dropout lists based on galaxy morphology (U -dropouts only) and rest-frame B -band luminosity. We used the CAS morphology system (Conselice 2003, hereafter C03) to divide the U -dropout list according to the observed-frame z_{850} -band (rest-frame $\lambda\lambda 2000-2500$) concentration and asymmetry parameters. We note that the CAS parameters have been derived using rest-frame UV light and may have somewhat different physical interpretations than those quoted for the local Universe. Concentration (C) is proportional to the logarithm of the ratio of the radii containing 80% and 20% of the source flux:

$$C = 5 \times \log (r_{80\%}/r_{20\%}) \quad (6)$$

Galaxies with high C values (e.g., bulge dominated systems locally) are generally brightest in their central regions (Conselice, Gallagher, & Wyse 2002). Asymmetry (A) is defined for a galaxy by taking the absolute value of the difference in fluxes of the galaxy's image and its 180° rotated analog and dividing by the original image flux (see Conselice, Bershady, & Jangren 2000; C03, for details). Generally disk-dominated systems and galaxy mergers are observed to have high A values in the local Universe. Parameter values of $A = 0.1$ and $C = 2.7$ were chosen to divide the U -dropout list roughly in half, resulting in lists of LBGs with $A < 0.1$, $A > 0.1$, $C < 2.7$, and $C > 2.7$.

We also divided our original dropout lists into subsets based on rest-frame B -band luminosity. Rest-frame B -band luminosities were calculated using a spectral energy distribution (SED) and applying K -corrections to the fluxes (e.g., Schneider, Gunn, & Hoessel 1983; Hogg 2002). K -corrected ACS magnitudes

were used in these computations, thus the derived rest-frame B -band luminosities are strongly dependent on the SED choice. An SED for LBGs was used in calculating K -corrections. This SED was derived from the Bruzual & Charlot (2003) solar metallicity models, with a Salpeter initial mass function, and aged by 144 Myr at constant SFR. Optically bright and faint sublists were generated by dividing each dropout list (i.e., U -, B_{435} -, V_{606} -, and i_{775} -dropouts) at its mean rest-frame B -band luminosity. The corresponding mean rest-frame B -band luminosities used in these divisions were $L_B \approx 5.3, 5.5, 4.1$, and 5.5×10^{43} erg s $^{-1}$ ($M_B \approx -20.6, -20.5, -20.1, -20.6$) for U -, B_{435} -, V_{606} -, and i_{775} -dropouts, respectively. Because rest-frame B -band luminosity distributions are asymmetric with skew tails toward high luminosity, splitting at the mean leads to two lists with unequal sizes.

3. Results

3.1. Detected Sources

Over the GOODS fields seven U -dropouts, eight B_{435} -dropouts, two V_{606} -dropouts, and one i_{775} -dropout were found to be coincident with *Chandra* sources within the positional errors (see Table 1).² Positional errors, photon counts, effective photon indices, and fluxes for these sources were determined in A03. The 2.0–8.0 keV X-ray luminosities were computed using eqn. 5.³ We investigated the probability of obtaining a false match by shifting all of our LBG positions and checking to see if the new positions were coincident with *Chandra* sources. LBG positions were shifted by 10'' in 16 different directions, and an average of ≈ 2 detections were obtained for each direction.

Of the 18 detected sources, we find that 14 have corresponding spectroscopic (Barger et al. 2003a; Cristiani et al. 2004; Szokoly et al. 2004) and/or photometric (Barger et al. 2003a; Mobasher et al. 2004; Zheng et al. 2004) redshifts. Of these 14 sources, four (J123621.0+621412, J123642.2+620612, J123701.6+621146, J033243.2–274914) have redshifts inconsistent with those determined by the Lyman break technique. We note that the redshifts derived for three of the four sources (J123621.0+621412, J123642.2+620612, and J123701.6+621146) are photometric redshifts, implying there are still uncertainties in their values. These may perhaps be dismissed as being “inconsistent.” The spectroscopic redshift of $z = 1.92$ for U -dropout J033243.2–274914 would therefore be the only remaining discrepant case. This LBG may be an interloper (see § 2.1 for probabilities) or falsely matched. Furthermore, the colors of some AGN may satisfy the color criteria used to select normal galaxies of differing redshifts. This may cause a discrepancy between spectroscopic and color-selected redshifts derived for these AGN.

The detected sources are mostly AGN with moderate luminosities (i.e., $L_X \approx 10^{43}–10^{44.5}$ erg s $^{-1}$),

²Note that the Lyman break technique is a statistical process for isolating galaxies at a given redshift. Due to the statistical nature of this process, we do not expect to recover all objects within the ACS flux limits that may reside at the redshifts under investigation here.

³For reference, the on-axis sensitivity limit for the 2 Ms CDF-N is $\approx 2.5 \times 10^{-17}$ erg cm $^{-2}$ s $^{-1}$ in the soft band corresponding to rest-frame 2.0–8.0 keV luminosities of 2.0, 4.0, 6.8, and 10.4×10^{42} erg s $^{-1}$ at $z = 3, 4, 5$, and 6, respectively ($\Gamma = 2$).

characteristic of luminous Seyfert type galaxies to quasars. Several of these sources have been characterized in previous investigations. J123648.0+620941 is the highest redshift quasar known ($z = 5.186$) in the CDF-N and -S fields (e.g., Barger et al. 2003b; Vignali et al. 2002). J033201.6–274327, J033218.2–275241, J033243.2–274914, J033244.3–275251 (Szokoly et al. 2004), and J033209.4–274807 (Schreier et al. 2001) have been spectroscopically classified as broad-line AGN. J123701.6+621146 and J123647.9+620941 are both Very Red Objects ($I-K \geq 4$, VROs; Alexander et al. 2002a). J033229.8–275105 has been identified as a putative type 2 QSO (Norman et al. 2002). Finally, three additional sources (J033239.7–274851, J033242.8–274702, and J033250.2–275252) have been cataloged as high-redshift QSO candidates (Cristiani et al. 2004).

Following Alexander et al. (2002b) we assume detected sources with $2.0\text{--}8.0 \text{ keV } L_X > 1.5 \times 10^{42} \text{ erg s}^{-1}$ or $\Gamma < 1.0$ are AGN. Only one source (J123642.2+620612) falls outside these criteria, leaving 17 clear AGN. The derived AGN fractions for our U -, B_{435} -, V_{606} -, and i_{775} -dropouts are $\approx 1.2\%$, 0.4% , 0.3% , and 0.4% , respectively; these fractions are lower than others found in previous investigations. For comparison, the AGN fraction derived from N02 is $\approx 2.7\%$. In comparison to our B_{435} -, V_{606} -, and i_{775} -dropouts, our U -dropouts and the LBGs used by N02 are relatively luminous in the optical. The corresponding AGN fractions therefore suggest X-ray luminous AGN are generally optically luminous as well.

3.2. Stacked Sources

The results of our stacking analyses of individually undetected sources are found in Table 2. Hereafter, unless stated otherwise, we discuss the results in reference to the soft-band stacking analyses where we obtain significant detections; we do not obtain significant detections in the hard- or full-bands (this result is understandable due to the significantly lower background in the soft-band). The stacking procedure was repeated for the GOODS-N and GOODS-S fields individually; results from the two fields were statistically consistent. Generally, we detect the stacked emission from U -dropouts ($\sim 7\sigma$) and all subsets generated therefrom. We do not obtain significant detections ($S/N > 3\sigma$) for general samples of B_{435} -, V_{606} -, and i_{775} -dropouts, but we note a suggestive positive fluctuation ($\sim 2\sigma$) for our B_{435} -dropouts. We do, however, obtain a significant detection for the bright subset of B_{435} -dropouts ($\sim 3\sigma$). Figure 3a shows the distributions of counts obtained for the individual galaxies being stacked for both U -dropouts and the bright subset of B_{435} -dropouts. We obtained an average of 3.1 and 2.3 counts per cell for U - and bright B_{435} -dropouts, respectively. The summed numbers of source plus background counts were 1351 counts for U -dropouts and 926 for bright B_{435} -dropouts. In the 10,000 Monte Carlo trials where we shifted the aperture cells to random positions and summed background counts, we found that no trials produced $\gtrsim 1351$ counts for U -dropouts and only 6 trials produced $\gtrsim 926$ counts for B_{435} -dropouts. Gaussian statistics predict ≈ 0 and 5 Monte Carlo trials should exceed the total source plus background counts for our analysis of U -dropouts and bright B_{435} -dropouts, respectively. Figure 3b shows the Monte Carlo distributions obtained when stacking random positions over 10,000 trials. In both cases the detection confidence levels are greater than 99.9%. Stacked and smoothed images are displayed in Figure 4. The images have effective exposure times of ≈ 0.7 and 0.5 Gs (22 and 16 yr) for U - and bright B_{435} -dropouts, respectively.

Stacked V_{606} - and i_{775} -dropouts and subsets thereof produced no significant detections (i.e., $S/N < 3\sigma$). We also attempted to merge the bright subsets of V_{606} -dropouts and i_{775} -dropouts and failed to obtain detections. X-ray emission constraints for these LBGs are tabulated in Table 2.

4. Discussion

Using the ≈ 2 Ms CDF-N plus ≈ 1 Ms CDF-S we have placed constraints on the X-ray properties of LBGs identified in the 316 arcmin 2 GOODS-N and -S fields. We have used X-ray stacking techniques on samples of 449, 1734, 629, and 247 individually undetected LBGs at $z \sim 3, 4, 5$, and 6, respectively (U -, B_{435} -, V_{606} -, and i_{775} -dropouts, respectively) to obtain their average X-ray properties. X-ray emission from LBGs is expected to be largely due to activity associated with star-forming processes (e.g., HMXBs and young supernova remnants) with a low-level contribution from low-luminosity AGN (LLAGN; e.g., Ho et al. 2001). With the intent to investigate normal/starburst galaxies we have rejected LBGs coincident with known *Chandra* sources from our stacking analyses. Considering *Chandra*'s superb sensitivity for detecting luminous AGN, we are confident that this rejection process has effectively removed strong accretion-dominated X-ray sources that would heavily contaminate our stacked signal. We have identified 18 LBGs coincident with *Chandra* sources (see § 3.1). With the possible exception of one source we find these objects are moderately luminous AGN comprising $\approx 0.5\%$ of the LBG population from $z \sim 3-6$.

Using our stacking procedure (see § 2) we detect X-ray emission from LBGs at $z \sim 3$ and an optically bright subset of LBGs at $z \sim 4$. X-ray count rates derived from our soft-band detections and hard-band upper limits (3σ) were used to constrain the spectral slopes of these LBGs. The 2.0–8.0 keV to 0.5–2.0 keV band ratio ($\Phi_{2.0-8.0\text{ keV}}/\Phi_{0.5-2.0\text{ keV}}$) is calculated to be < 0.9 for U -dropouts corresponding to an effective photon index lower limit of $\Gamma > 0.8$; a consistent, less tightly constrained photon index is also derived for our bright B_{435} -dropouts. This lower limit is consistent with our assumed $\Gamma = 2$ photon index, which is expected for galaxies with high star formation activity. The derived average 2.0–8.0 keV X-ray luminosities for these LBGs are ≈ 1.5 and 1.4×10^{41} erg s $^{-1}$ for U -dropouts and bright B_{435} -dropouts, respectively, a factor of $\approx 5-10$ times higher than for typical starburst galaxies in the local Universe (e.g., M 82; Griffiths et al. 2000). Furthermore, our LBGs are a factor of ≈ 2 less X-ray luminous than those studied by B01 and N02.

Assuming the X-ray luminosity functions of our individually undetected LBGs at high redshifts have similar functional forms to those of normal/starburst galaxies in the local Universe, we can estimate the expected median X-ray luminosities for these LBGs. This is important because, for a luminosity function with significant skewness, the median will differ from the mean. We have investigated this using the David, Jones, & Forman (1992, hereafter DJF92) sample of 71 normal/starburst galaxies in the local Universe and find the mean to median X-ray luminosity ratio $L_X^{\text{mean}}/L_X^{\text{median}} \approx 5$. The mean 2.0–8.0 keV X-ray luminosity for these 71 galaxies is $\approx 6 \times 10^{40}$ erg s $^{-1}$, a factor of ≈ 2.5 lower than the mean X-ray luminosities of our U -dropouts and optically bright subset of B_{435} -dropouts. If we assume the $L_X^{\text{mean}}/L_X^{\text{median}}$ ratio for our LBGs is similar to that of the DJF92 sample, the corresponding median 2.0–8.0 keV X-ray luminosity

would be $\approx 3 \times 10^{40}$ erg s $^{-1}$.

The strong U -dropout signal allows investigation of the contribution of specific subsets to the photon statistics (see § 2.2 for details and Table 2 for results). We find that the optically luminous U -dropouts contribute most of the X-ray flux ($S/N_{\text{bright}} \approx 1.5 \times S/N_{\text{dim}}$). It is possible that the emission from rest-frame UV may be heavily obscured by dust as would be expected if LBGs were a “scaled-up” population of ultraluminous infrared galaxies (ULIRGs; Goldader et al. 2002). The X-ray to B -band mean luminosity ratios for these LBGs suggests that this is likely not the case, and the intrinsic dust attenuation from LBGs is similar to that expected for star-forming galaxies (see Seibert et al. 2002). We find that relatively asymmetric sources ($A > 0.1$) dominate the photon counts. However, the rest-frame B -band luminosities of these LBGs are somewhat elevated as compared with sources of low-asymmetry index (i.e., $A \leq 0.1$), and we therefore offer no further interpretation. Furthermore, stacking of the two LBG subsets split by concentration index ($C > 2.7$ and $C \leq 2.7$) show that these two morphological subsets have similar X-ray properties. No additional information was extracted from our divisions on asymmetry and concentration.

Recent investigations have found that hard X-ray emission largely associated with HMXBs can be used as a direct indicator of SFR (e.g., Bauer et al. 2002; Ranalli, Comastri, & Setti 2003; Grimm, Gilfanov, & Sunyaev 2003; Persic et al. 2004). If we assume the majority of the X-ray emission from our stacked detections of U -dropouts and bright B_{435} -dropouts is unobscured X-ray emission from HMXBs, we expect the corresponding mean SFRs to be ≈ 85 – $240 M_{\odot}$ yr $^{-1}$. These SFRs were derived using the linear SFR– $L_{2-10 \text{ keV}}^{\text{HMXB}}$ relation given as equation (2) of Persic et al. (2004) assuming a correlation error of 20%. For comparison, the mean SFRs derived from the rest-frame 1500 Å fluxes are estimated to be ≈ 65 and $10 M_{\odot}$ yr $^{-1}$ for our U -dropouts and bright B_{435} -dropouts, respectively, without UV extinction. When a correction is made for dust extinction, the corresponding SFRs are ≈ 400 and $60 M_{\odot}$ yr $^{-1}$ (see G04). The reasonable agreement between the X-ray and UV extinction-corrected derived SFRs broadly supports our assumption that the X-ray emission is dominated by star-forming processes with little contribution needed from LLAGN.

The X-ray luminosities for star-forming galaxies (such as LBGs) are potential tracers of global star formation history (Lilly et al. 1996; Madau et al. 1996; Blain et al. 1999). A global estimate of the SFR can be implicitly drawn from these LBGs by considering the mean X-ray luminosity per mean B -band luminosity, L_X/L_B (mean quantities).⁴ This ratio should be interpreted with some caution due to the possible non-linear relationship between L_X and L_B (i.e. $L_X \propto L_B^{\alpha}$). The power-law index (α) for this relation has been reported to range from ≈ 1 (DJF92; Fabbiano & Trinchieri 1985) to as high as ≈ 1.5 (Shapley et al. 2001) for galaxies in the local Universe. We find that L_X/L_B shows suggestive evidence for evolution with redshift as illustrated in Figure 5a. Here our U -dropouts and bright B_{435} -dropouts are plotted and compared with the results for normal galaxies at $z \approx 0$ (DJF92) and early-type spirals from $z \approx 0.05$ – 1.5 (Wu et al. 2004). From these data we infer a peak in L_X/L_B at $z \approx 1.5$ – 3.0 , consistent with predictions of GW01. These results, while based on larger samples of galaxies, are consistent with the near constancy of L_X/L_{UV}

⁴In our stacking analyses we compute an average L_X for a given stack of source positions. We therefore refer to L_X/L_B as meaning $\langle L_X \rangle / \langle L_B \rangle$, where $\langle L_X \rangle$ and $\langle L_B \rangle$ are mean quantities. When necessary for comparisons, data regarding L_X/L_B have been converted to this form.

at $z \sim 1$ and $z \sim 3$ reported by N02 for Balmer break galaxies and LBGs, respectively. In this description the global SFR is expected to peak at $z \approx 2.5\text{--}3.5$. During this epoch, X-ray emission is observed due to contributions from HMXBs and supernovae. Shortly after the UV luminous population evolves, X-ray emission will continue in the form of LMXBs resulting in an increase in L_X/L_B .

When stacking LBGs at higher redshift, $z \sim 5$ and 6 (V_{606} - and i_{775} -dropouts, respectively), we do not obtain significant detections. The AGN contribution may be slightly more significant for these LBGs where the *Chandra* exposures are only capable of detecting individual objects with 2.0–8.0 keV luminosities $\gtrsim 10^{43}$ erg s $^{-1}$ (implying many Seyfert type AGN might not be individually detected at these redshifts). In light of these limits we therefore place constraints on the average AGN content of these LBGs. The derived rest-frame 2.0–8.0 keV luminosity upper limits (3σ) for the V_{606} - and i_{775} -dropouts are 2.8 and 7.1×10^{41} erg s $^{-1}$. Such upper limits are characteristic of bright starburst or low-luminosity Seyfert type galaxies and are the tightest constraints yet to be placed on the X-ray properties of LBGs at $z \gtrsim 5$. For comparison, X-ray analyses of 44 LBGs at $z \sim 5$ (Bremer et al. 2003) and 54 LBGs at $z \sim 6$ (Moustakas & Immler 2004) constrain their average 2.0–8.0 keV X-ray luminosities to be less than 3 and 7×10^{42} erg s $^{-1}$ (3σ), respectively.

Figure 5b shows the overall L_X/L_B vs L_X results for both individually detected and stacked LBGs. Stacking analyses show that the individually undetected LBGs at $z \sim 3, 4, 5$, and 6 have L_X/L_B ratios characteristic of local starburst galaxies. Our individually detected LBGs have much larger L_X/L_B ratios, which are expected for X-ray luminous AGN.

We gratefully acknowledge support from STScI grant HST-GO-09425.26-A and NSF CAREER award AST-9983783 (BDL,WNB), the Royal Society (DMA), and NSF grant 03-07582 (DPS). We thank Stefan Immler and Wentao Wu for useful discussions and development of software.

REFERENCES

Alexander, D. M., Vignali, C., Bauer, F. E., Brandt, W. N., Hornschemeier, A. E., Garmire, G. P., & Schneider, D. P. 2002a, AJ, 123, 1149

Alexander, D. M., Aussel, H., Bauer, F. E., Brandt, W. N., Hornschemeier, A. E., Vignali, C., Garmire, G. P., & Schneider, D. P. 2002b, ApJ, 568, L85

Alexander, D. M. et al. 2003, AJ, 126, 539 (A03)

Barger, A. J., et al. 2003, AJ, 126, 632

Barger, A. J., Cowie, L. L., Capak, P., Alexander, D. M., Bauer, F. E., Brandt, W. N., Garmire, G. P., & Hornschemeier, A. E. 2003, ApJ, 584, L61

Bauer, F. E., Alexander, D. M., Brandt, W. N., Hornschemeier, A. E., Vignali, C., Garmire, G. P., & Schneider, D. P. 2002, AJ, 124, 2351

Bauer, F. E., et al. 2004, in preparation

Blain, A. W., Smail, I., Ivison, R. J., & Kneib, J. P. 1999, MNRAS, 302, 632

Brandt, W. N. et al. 2001b, AJ, 558, L5 (B01)

Bremer, M. N., Lehnert, M. D., Waddington, I., Hardcastle, M. J., Boyce, P. J., & Phillipps, S. 2004, MNRAS, 347, L7

Bruzual, G. & Charlot, S. 2003, MNRAS, 344, 1000

Capak, P., et al. 2004, AJ, 127, 180

Cohen, J. G., Hogg, D. W., Blandford, R., Cowie, L. L., Hu, E., Songaila, A., Shopbell, P., & Richberg, K. 2000, ApJ, 538, 29

Conselice, C. J., Bershady, M. A., & Jangren, A. 2000, ApJ, 529, 886

Conselice, C. J., Gallagher, J. S., & Wyse, R. F. G. 2002, AJ, 123, 2246

Conselice, C. J. 2003, ApJS, 147, 1 (C03)

Cristiani, S. et al. 2004, ApJ, 600, L119

David, L. P., Jones, C., & Forman, W. 1992, ApJ, 388, 82

Dickinson, M., et al. 2004, ApJ, 600, L99

Fabbiano, G. & Trinchieri, G. 1985, ApJ, 296, 430

Fabbiano, G. & Shapley, A. 2002, ApJ, 565, 908

Ghosh, P., White, N. E. 2001, *ApJ*, 559, 97 (GW01)

Giacconi, R. et al. 2002, *ApJS*, 139, 369

Giavalisco, M. et al. 2004a, *ApJ*, 600, L93

Giavalisco, M. et al. 2004b, *ApJ*, 600, L103 (G04)

Goldader, J. D., Meurer, G., Heckman, T. M., Seibert, M., Sanders, D. B., Calzetti, D., & Steidel, C. C. 2002, *ApJ*, 568, 651

Griffiths, R. E., Ptak, A., Feigelson, E. D., Garmire, G., Townsley, L., Brandt, W. N., Sambruna, R., & Bregman, J. N. 2000, *Science*, 290, 1325

Grimm, H.-J., Gilfanov, M., & Sunyaev, R. 2003, *MNRAS*, 339, 793

Helou, G., Ryter, C., & Soifer, B. T. 1991, *ApJ*, 376, 505

Ho, L. C. et al. 2001, *ApJ*, 549, L51

Hogg, D. W. 2000, *astro-ph/9905116*

Hogg, D. W. 2002, *astro-ph/0210394*

Hornschemeier, A. E. et al. 2002, *ApJ*, 568, 82 (H02)

Kaaret, P. et al. 2001, *MNRAS*, 321, L29

Kim, D. W., Fabbiano, G., & Trinchieri, G. 1992, *ApJ*, 393, 134

Lilly, S. J., Le Fevre, O., Hammer, F., & Crampton, D. 1996, *ApJ*, 460, L1

Lockman, F. 2003, *Soft X-ray Emission from Clusters of Galaxies and Related Phenomena*, ed. R. Lieu, in press, *astro-ph/0311386*

Madau, P., Ferguson, H., Dickinson, M., Giavalisco, M., Steidel, C., & Fruchter, A. 1996, *MNRAS*, 283, 1388

Malhotra, S., Wang, J. X., Rhoads, J. E., Heckman, T. M., & Norman, C. A. 2003, *ApJ*, 585, L25

Moustakas, L. A., Immler, S., 2004, *ApJ*, in press, *astro-ph/0405270*

Mobasher, B., et al. 2004, *ApJ*, 600, L167

Nandra, K., et al. 2002, *AJ*, 576, 625 (N02)

Norman, C., et al. 2002, *ApJ*, 571, 218

Persic, M., Rephaeli, Y., Braito, V., Cappi, M., Della Ceca, R., Franceschini, A., & Gruber, D. E. 2004, *A&A*, 419, 849

Ptak, A., Serlemitsos, P., Yaqoob, T., & Mushotzky, R. 1999, *ApJS*, 120, 179

Reddy, N. A. & Steidel, C. C. 2004, *ApJ*, 603, L13

Ranalli, P., Comastri, A., & Setti, G. 2003, *A&A*, 399, 39

Schmidt M. & Green, R. 1986, *ApJ*, 305, 68

Schneider, D. P., Gunn, J. E., & Hoessel, J. G. 1983, *ApJ*, 264, 337

Schreier, E. J., et al. 2001, *ApJ*, 560, 127

Seibert, M., Heckman, T. M., & Gerhardt, M. R. 2002, *ApJ*, 124, 46

Shapley, A. E., Fabbiano, G., Eskridge, P. B. 2001, *ApJ*, 137, 139

Shapley, A. E., Steidel, C. C., Pettini, M., & Adelberger, K. L. 2003, *ApJ*, 588, 65

Spergel, D. N., et al. 2003, *ApJS*, 148, 175

Stark, A. A., Gammie, C. F., Wilson, R. W., Bally, J., Linke, R. A., Heiles, C., & Hurwitz, M. 1992, *ApJS*, 79, 77

Steidel, C. C., Pettini, M., & Hamilton, D. 1995, *AJ*, 110, 2519

Steidel, C. C., Giavalisco, M., Dickinson, M., & Adelberger, K. L. 1996, *AJ*, 112, 352

Steidel, C. C., Adelberger, K. L., Giavalisco, M., Dickinson, M., & Pettini, M. 1999, *ApJ*, 519, 1

Szokoly, G. P., et al. 2004, *ApJ*, in press, astro-ph/0312324

Vignali, C., Bauer, F. E., Alexander, D. M., Brandt, W. N., Hornschemeier, A. E., Schneider, D. P., & Garmire, G. P. 2002, *ApJ*, 580, L105

Wang, J. X., et al. 2004, *ApJ*, in press, astro-ph/0404611

Wu, W., et al. 2004, in preparation

Zheng, W., et al. 2004, *ApJ*, in press, astro-ph/0406482

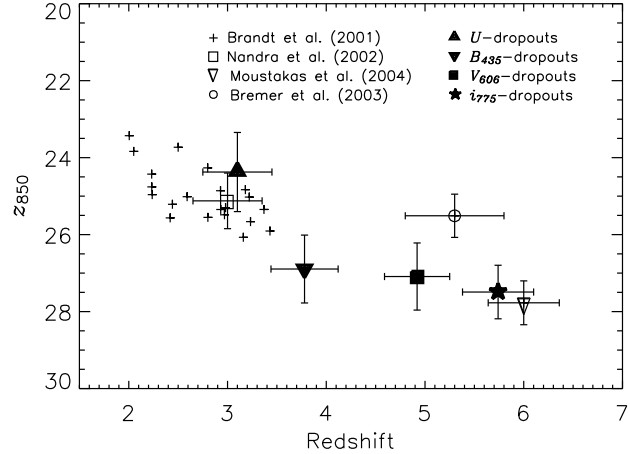


Fig. 1.— z_{850} magnitude vs. redshift for X-ray stacking analyses of LBGs. Filled (our LBGs) and open symbols (other investigations) represent the estimated mean z_{850} and redshift with error bars showing the 1σ spread for each quantity. The Brandt et al. (2001) measurements (+) represent the positions of individual LBGs with spectroscopic redshifts.

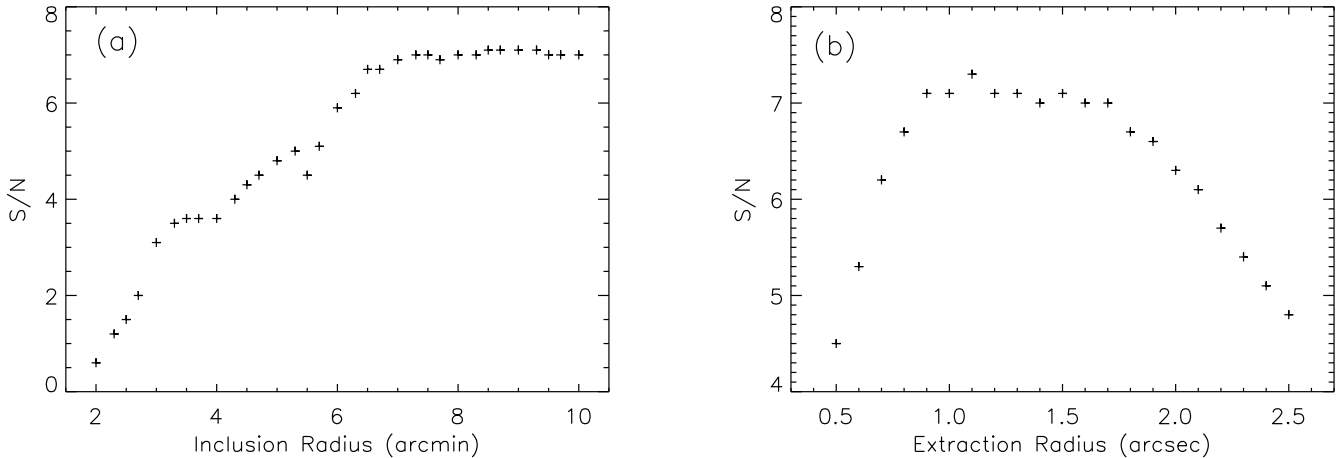


Fig. 2.— (a) The achieved signal-to-noise ratio (S/N) as a function of inclusion radius for stacking U -dropouts. Note that the number of stacked sources rises with increasing inclusion radius and is maximized at ≈ 9.0 . (b) Signal-to-noise ratio (S/N) as a function of extraction radius. Here, the signal is strongest for an aperture radius of $\approx 1.5''$. This process of optimizing the S/N was achieved iteratively and appears here in convergence.

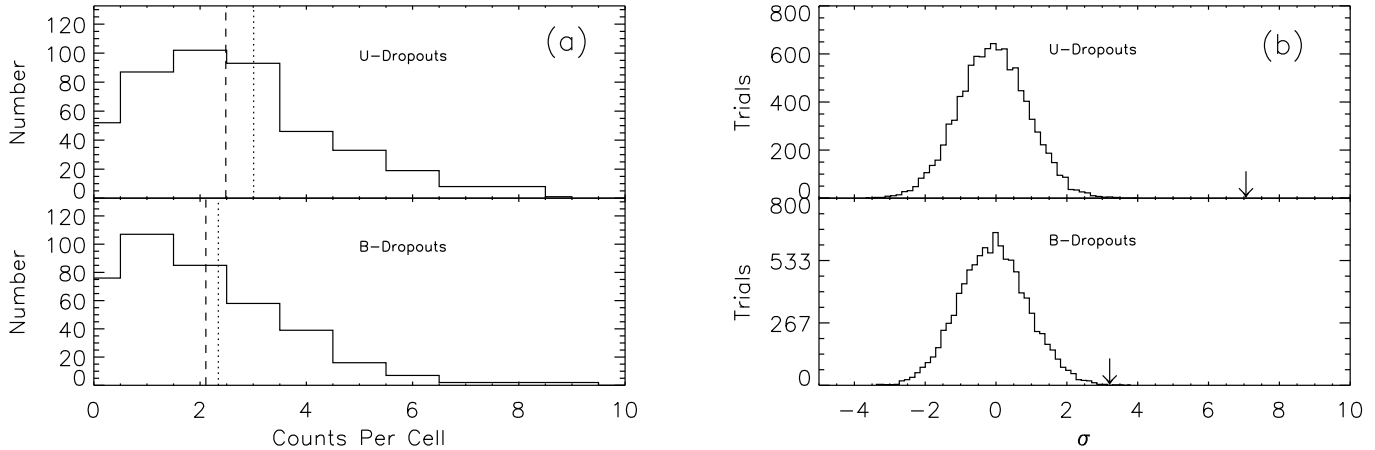


Fig. 3.— (a) Histogram of the count distribution for U -dropouts (upper panel) and B_{435} -dropouts (lower panel). The vertical dotted lines show the mean source plus background counts per aperture cell, and the vertical dashed lines show the mean background counts per aperture cell. (b) Results from Monte Carlo estimates of the background level for U -dropouts (upper panel) and B_{435} -dropouts (lower panel). The detection level is represented with downward pointing arrows.

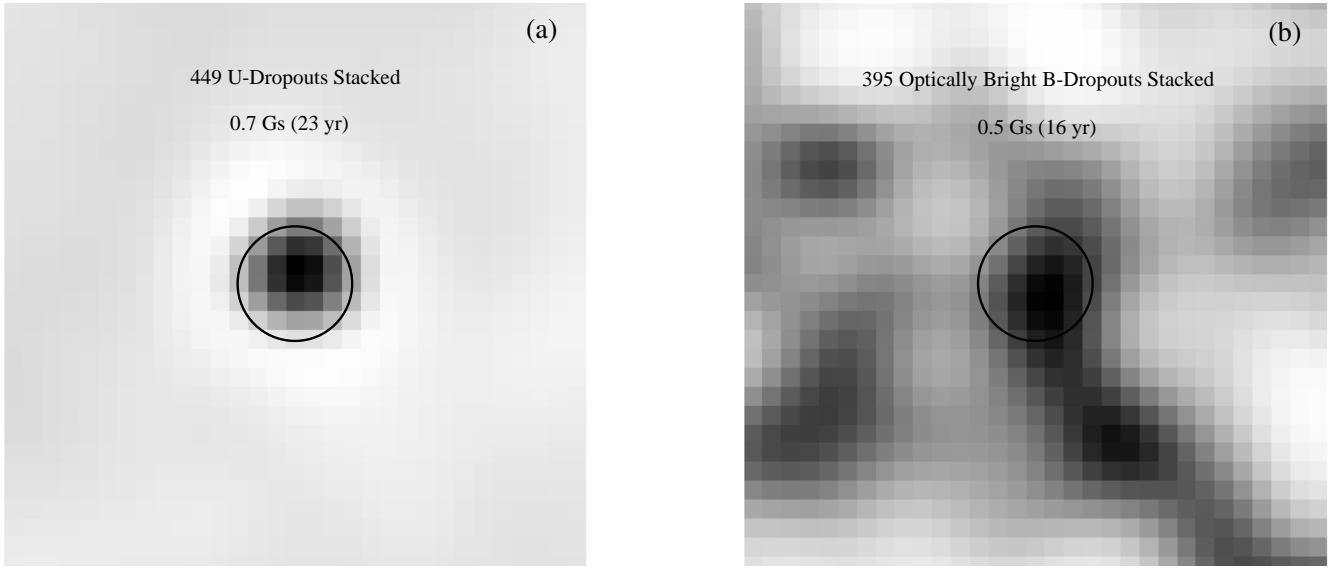


Fig. 4.— Stacked soft-band images of 449 U -dropouts (≈ 0.7 Gs exposure) and 395 optically bright B_{435} -dropouts (≈ 0.5 Gs exposure). Stacked emission from these LBGs is significantly detected in the soft-band with significances of $\sim 7\sigma$ (U -dropouts) and $\sim 3\sigma$ (bright B_{435} -dropouts). The images are $15'' \times 15''$ (0.5 pixel $^{-1}$) and were adaptively smoothed at 2.5σ using the CIAO tool CSMOOTH. The faint “nebulosity” observed in the optically bright B_{435} -dropouts is attributed to smoothing over noise. The black circles are centered on our $1.5''$ radius aperture cell that was used in the stacking analyses.

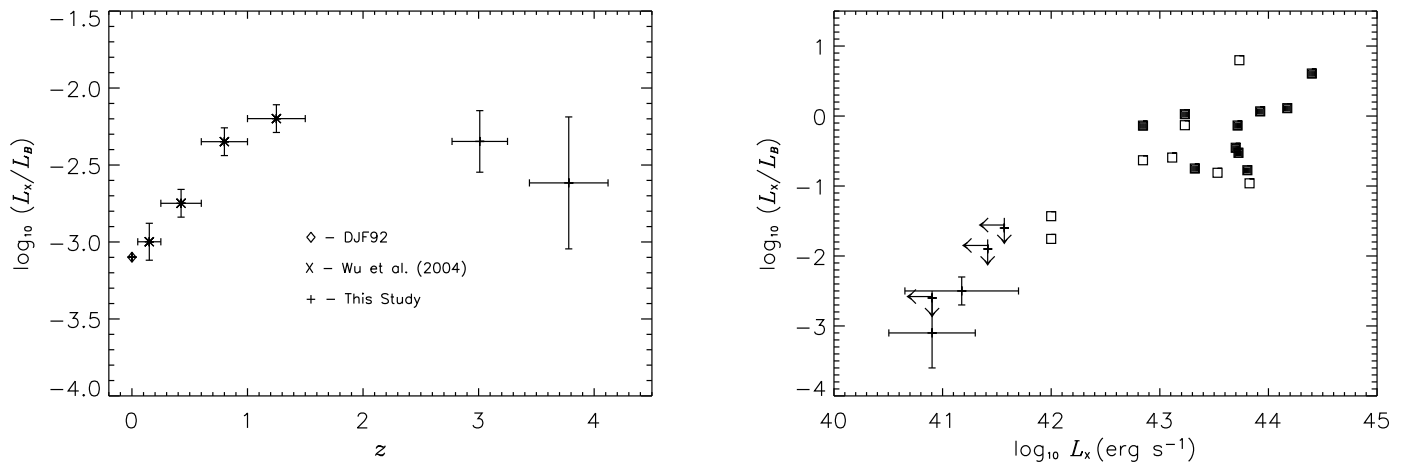


Fig. 5.— (a) The X-ray (0.5–4.5 keV) to B -band luminosity ratio vs. redshift. Note the suggested maximum of L_X/L_B at $z \sim 1.5$ –3 is consistent with predictions from the cosmic star formation history. Data used in this figure come from the following sources: $z \sim 0$ (DJF92), $z \sim 0.05$ –1.5 (Wu et al. 2004), $z \sim 3$ and 4 – our U -dropouts and B_{435} -dropouts, respectively. (b) X-ray to B -band luminosity ratio vs. X-ray luminosities of individually undetected stacked LBGs (+) and individually detected LBGs (\square); solid squares represent broad-line AGN. The individually detected sources are AGN (with one possible exception) and have much larger L_X/L_B ratios than our stacked LBGs. X-ray luminosities were calculated assuming a power law with photon index $\Gamma = 2$, and B -band luminosities were computed using K -corrections with an LBG SED (see § 2.2).

Table 1. Individually Detected LBGs

<i>Chandra</i> Name J2000 (1)	Dropout Bandpass (2)	Pos. Er. (arcsec) (3)	Offset (arcsec) (4)	z (5)	Counts SB (6)	$f_{0.5-2 \text{ keV}}$ ($\times 10^{-16}$ erg cm $^{-2}$ s $^{-1}$) (7)	$f_{2-8 \text{ keV}}$ ($\times 10^{-16}$ erg cm $^{-2}$ s $^{-1}$) (8)	Γ (9)	$L_{2-8 \text{ keV}}$ ($\times 10^{43}$ erg s $^{-1}$) (10)	z_{850} (11)
J033201.6-274327	<i>U</i>	0.4	0.15	2.726 ^s	450.7	27.7	56.2	1.5	14.9	23.8
J033209.4-274807	<i>U</i>	0.3	0.10	2.81 ^s	195.6	11.0	59.7	0.8	6.4	22.4
J033218.2-275241	<i>U</i>	0.6	0.10	2.801 ^s	55.9	3.6	6.3	1.6	2.1	24.1
J033222.2-274937	<i>B</i> ₄₃₅	0.6	0.19	—	10.1	0.6	< 3.8	1.4	0.7	27.5
J033229.8-275106	<i>B</i> ₄₃₅	0.6	0.14	3.700 ^s	53.5	3.1	31.8	0.4	3.4	24.8
J033238.8-275122	<i>B</i> ₄₃₅	0.6	0.25	—	16.2	1.1	8.9	0.6	1.3	26.3
J033239.1-274439	<i>B</i> ₄₃₅	0.6	0.24	—	76.2	4.6	21.0	0.9	5.4	28.0
J033239.7-274851	<i>B</i> ₄₃₅	0.3	0.14	3.064 ^s	134.6	7.5	7.1	0.4	5.3	24.8
J033242.8-274702	<i>B</i> ₄₃₅	0.6	0.13	3.193 ^s	112.0	6.3	16.4	1.3	5.0	25.2
J033243.2-274914	<i>U</i>	0.3	0.02	1.92 ^s	621.4	36.6	61.1	1.7	8.4	24.2
J033244.3-275251	<i>U</i>	0.7	0.29	3.471 ^s	85.4	5.4	6.8	1.9	5.2	24.2
J033250.2-275252	<i>B</i> ₄₃₅	0.4	0.33	3.6 ^p	404.2	24.0	75.3	1.2	25.1	26.1
J123621.0+621412	<i>U</i>	0.6	0.16	1.74 ^p	131.9	3.7	6.0	1.7	0.7	25.4
J123642.2+620612	<i>B</i> ₄₃₅	0.4	0.39	0.70 ^p	126.4	3.9	12.6	1.2	0.1	26.4
J123647.9+621020	<i>V</i> ₆₀₆	0.6	0.26	—	28.1	0.8	19.4	> 0.3	1.7	27.3
J123648.0+620941	<i>V</i> ₆₀₆	0.6	0.23	5.186 ^s	96.7	2.7	4.9	1.6	6.7	23.8
J123701.6+621146	<i>i</i> ₇₇₅	0.6	0.43	1.52 ^p	13.9	0.4	< 1.2	1.4	0.1	27.8
J123714.3+621208	<i>U</i>	0.6	0.14	3.146 ^s	74.0	2.2	5.2	1.4	1.7	25.5

Note. — Col.(1): *Chandra* source name. Col. (2): Observed ACS dropout bandpass. Col.(3): Positional error as reported in A03. Col.(4): Angular offset between positions determined by *Chandra* and ACS. Col.(5): Spectroscopic (“s” superscript) or photometric (“p” superscript) redshift. Col.(6): Soft-band X-ray counts. Col.(7): Soft-band flux. Col.(8): Hard-band flux. Col.(9): Effective photon index. Here a value of 1.4 was assumed when photon statistics were too low to determine accurate values. Col.(10): Hard-band X-ray luminosity. Col.(11): z_{850} -band magnitude.

Table 2. Stacking Results For Filtered Dropout Lists

Data Type	<i>N</i>	<i>S</i>	<i>B</i>	σ	S/N	E(Ms)	<i>N</i> _{trials > S}	Φ (10^{-7} counts s ⁻¹)	f_X (10^{-18} erg cm ⁻² s ⁻¹)	L_X (10^{41} ergs s ⁻¹)	L_B (10^{43} ergs s ⁻¹)	$\log(L_X/L_B)$
(1)	(2)	(3)	(4)	(5)	(6)	(7)	(8)	(9)	(10)	(11)	(12)	(13)
<i>U</i>-dropouts ($z \sim 3$)												
General	449	1351.0	1115.3	33.4	7.1	663.9	0	3.6 ± 0.7	1.9 ± 0.4	1.5 ± 0.3	5.3	-2.6 ± 0.2
Bright	201	589.2	462.4	21.5	5.9	274.8	0	4.6 ± 1.2	2.4 ± 0.6	1.9 ± 0.5	10.3	-2.7 ± 0.3
Dim	248	759.7	651.9	25.5	4.2	389.2	0	2.8 ± 1.0	1.5 ± 0.5	1.2 ± 0.4	3.1	-2.4 ± 0.3
$C > 2.7$	223	672.0	559.4	23.7	4.8	332.7	0	3.4 ± 1.1	1.8 ± 0.6	1.4 ± 0.4	4.5	-2.5 ± 0.3
$C \leq 2.7$	226	676.8	555.2	23.6	5.2	331.2	0	3.7 ± 1.1	1.9 ± 0.6	1.5 ± 0.4	6.1	-2.6 ± 0.3
$A > 0.1$	213	671.3	524.1	22.9	6.4	312.7	0	4.7 ± 1.1	2.5 ± 0.6	2.0 ± 0.5	6.7	-2.5 ± 0.2
$A \leq 0.1$	236	677.5	591.0	24.3	3.6	351.2	0	2.5 ± 1.0	1.3 ± 0.5	1.0 ± 0.4	4.3	-2.6 ± 0.4
<i>B</i>₄₃₅-dropouts ($z \sim 4$)												
General	1734	3749.5	3625.7	60.2	2.1	2102.2	197	$\lesssim 1.2$	$\lesssim 0.6$	$\lesssim 0.9$	2.9	$\lesssim -2.4$
Bright	395	925.5	832.9	28.9	3.2	485.5	6	1.9 ± 0.9	1.0 ± 0.5	1.4 ± 0.6	9.2	-2.8 ± 0.5
Dim	1339	2823.8	2793.6	52.9	0.6	1616.8	2783	$\lesssim 1.4$	$\lesssim 0.7$	$\lesssim 1.0$	2.1	$\lesssim -2.7$
<i>V</i>₆₀₆-dropouts ($z \sim 5$)												
General	629	1382.0	1373.7	37.1	0.2	804.9	4067	$\lesssim 2.0$	$\lesssim 1.0$	$\lesssim 2.8$	2.6	$\lesssim -2.8$
<i>i</i>₇₇₅-dropouts ($z \sim 6$)												
General	247	533.3	505.5	22.5	1.2	296.0	1065	$\lesssim 3.3$	$\lesssim 1.7$	$\lesssim 7.1$	3.7	$\lesssim -1.8$

Note. — The data apply to stacking analyses in the soft band. Col.(1): Description of the LBG sample stacked. “Bright” and “Dim” subsets were created by splitting the “General” lists at rest-frame B -band luminosities ≈ 5.3 and 5.5×10^{43} erg s $^{-1}$ ($M_B \approx -20.6$ and -20.5) for U -dropouts and B_{435} -dropouts, respectively. Col.(2): Number of sources being stacked. Col.(3): X-ray source counts obtained from stacking. Col.(4): Mean background counts obtained from Monte Carlo simulations. Col.(5): Poisson error of the background $B^{0.5}$. Col.(6): Signal-to-noise ratio $(S-B)/B^{0.5}$. Col.(7): Total, stacked effective exposure time. Col.(8): Number of Monte Carlo trials (out of 10,000) that produced a background estimate $> S$. Col.(9): X-ray count rate. Col.(10): X-ray (0.5–2.0 keV) flux. Col.(11): 2–8 keV rest-frame luminosity. Col.(12): Rest-frame B -band luminosity. Col.(12): Logarithm of X-ray to B -band luminosity ratio.